Near-infrared light-driven Janus nanomotors for deep tumor penetration and enhanced tumor immunotherapy

Ke Ma, Zelong Chen, Kai Liang, Yuxin Pei and Zhichao Pei*

Shaanxi Key Laboratory of Natural Products & Chemical Biology, College of Chemistry & Pharmacy, Northwest A&F University, Yangling 712100, P. R. China.

Supporting Information

1. Instrumentation

All reagents were purchased from commercial suppliers and used without further purification. The water used in this work was triple distilled. DLS measurements were performed on ZEN3600 NANOPHOX (MALVERN INSTRUMENTS LIMITED, United Kingdom). UV-vis spectra were collected with (Shimadzu UV-2450, Japan) UV-visible spectrophotometer. Scanning electron microscopy (SEM) images were obtained from the Nano SEM-450 instrument (FEI Ltd. U.S.A.). Transmission electron microscopy (TEM) images were obtained from the TECNAI G2 SPIRIT BIO instrument (FEI Ltd. U.S.A.). Cell culture was carried out in an incubator with a humidified atmosphere of 5% CO_2 at 37℃. The confocal laser microscope (CLSM) data were acquired using a Spectroscopic fluorescent lifetime Confocal Laser Scanning Microscopy STELLARIS8 FALCON (Lecia Instrument Co., LTD, Germany). The other fluorescent images were from the DMi8 Inverted fluorescence microscope (Leica MICROSYSTEMS, Germany). Flow cytometry data were obtained from BD FACSAria™ III Flow Cytometer (BD Biosciences, U.S.A.).

2. Live subject statement

All experiments were performed in accordance with the International Ethical Guidelines for Biomedical Research Involving Human Subjects of World Health Organization, and approved by the Northwest A&F University Animal Care Committee.

3. Synthesis of AMM-Col

Gold nanorods (AuNRs) were synthesized using a sodium oleate-assisted method[1]. The gold seed was prepared first: CTAB (0.739 g) was dissolved in 18.5 mL of ultrapure water and stirred for 10 min at 30 °C. Then, $HAuCl_4$ (10 mM, 0.5 mL) was added and stirred for 5 min. An ice-water solution containing $NaBH_4$ (9.1 mg, 20 mL) was prepared, and 1 mL of this solution was quickly added to the above mixture under vigorous stirring. When the solution changed from bright yellow to dark brown, the stirring was stopped after 2 min and the solution was left for 2 h. The AuNRs was subsequently carried out. CTAB (490 mg) and sodium oleate (86.5 mg) were dissolved in 33.6 mL of ultrapure water and stirred at 50 °C for 30 min. After the solution was cooled down to room temperature, $AgNO_3$ (4 mM, 1.2 mL) was added and stirred for 5 min and then left for 15 min at 30 °C. $HAuCl_4$ (10 mM, 1.75 mL) was added to the above solution and stirred for more than 30 min until the solution changed from bright yellow to colorless. Hydrochloric acid (36-38%, 100 μL) was added and stirred for 15 min, followed by adding ascorbic acid (56 μL) and stirring for 1 min. Finally, gold seed solution (28 μL) was added to the above solution and stirred for 1 min, resting overnight in a water bath at 30°C to obtain AuNRs. The 400, 600, and 800 μL of aqueous AuNRs solution (1

mg/mL) to add 300, 500, and 700 μL of aqueous collagenase solution (1 mg/mL), respectively, then 100 μL of aqueous PEG-SH solution (1 mg/mL) were added. After gently stirring for 24 h at 37 °C, washing with ultrapure water three times to obtain collagenase-coated AuNRs (AuNRs @Col)[2].

Tetrasulfur-bonded mesoporous organosilica nanoparticles (MONs) were prepared by adding CTAB (80 mg) to a mixture of ethanol (30 mL) and ultrapure water (130 mL), then adding 1 mL of concentrated ammonia (25 wt%) and continuing stirring for 1 h at 35°C until the solution changed from turbid to clear. TEOS (0.19 mL) and TESPTS (0.01 mL) were then added and stirred for 24 h. The white precipitate was collected by centrifugation and dispersed in an ethanol solution (80 mL) containing 40 μL of concentrated hydrochloric acid (36-38%), and refluxed with stirring at 60 °C for 12 h to remove the CTAB. Subsequently, the white precipitate was collected and dispersed in a mixture of ethanol (40 mL) and ultrapure water (2 mL), and 1 mL of glacial acetic acid and 200 μL of APTES were added and stirred at room temperature for 24 h. The precipitate was collected and washed with ethanol to obtain MONs-NH_2[3,4].Chitosan-unctionalized MONs (MONs@CS) were prepared by mixing 5 mL of the above MONs-NH_2 ethanol solution (1 mg/mL) with 5 mL of genipin ethanol solution (1 mg/mL) at room temperature for 3 h. The precipitates were collected and washed with ethanol, then dispersed in ultrapure water. 10 mL of the solution (1 mg/mL) and 2 mL of chitosan aqueous solution (1 mg/mL) were stirred at room temperature for 6 h. The precipitates were collected and washed to obtain MONs@CS[5].

Table S1. The mixing ratios of MONs@CS-Mn and AuNRs@Col (w/w).

MONs@CS-Mn/AuNRs@Col (w/w)	Size (nm)	PDI
5/0.5	172.9±3.2	0.354±0.047
5/1	234.0±2.9	0.262±0.014
5/1.5	173.4±10.1	0.655±0.165
5/2	199.9±1.4	0.639±0.063

AuNRs@Col-Mn-MONs@CS (AMM-Col) was fabricated via Mn^{2+} mediated ion-ligand interactions between AuNRs@Col and MONs@CS according to previous literature [6]. Taking 10 mL of MONs@CS aqueous solution (0.5 mg/mL, pH ~ 7) and 100 μL of $MnCl_2$ (0.1 mM) to stir at room temperature for 2 h. The precipitate was collected and washed with ultrapure water to disperse in ultrapure water to prepare MONs@CS-Mn aqueous solution. 10 mL of MONs@CS-Mn aqueous solution (0.5 mg/mL) and 1 mL of AuNRs@Col aqueous solution with various concentration (pH ~ 7) were stirred at room temperature for 2 h. The resultant solid was collected and washed with

ultrapure water to prepare AMM-Col. The mixing ratios of MONs@CS-Mn and AuNRs@Col was investigated by DLS. As shown in Table S1, the optimal mixing ratio is 5/1 owning to minimum polydispersity index (PDI). And the Janus morphology was identified through TEM (Fig. 1a).

4. The coupling rate of collagenase as well as DOX loading content and encapsulation rate

AuNRs@Col were prepared via dispersing AuNRs, collagenase and PEG-SH in water with the ratio of 8:7:1. After gently stirring at 37 °C for 24 h, the supernatant and precipitate were collected, where the uncoated collagenase in the supernatant was determined using the BCA method. Ploting the standard curve of collagenase in water and calculating the coupling efficiency (Coupling efficiency, %) of collagenase in AMM-Col. The calculation equation was as follows[7]:

$$\text{Coupling efficiency} = \frac{m_{(\text{the total of Col})} - m_{(\text{the supernant of Col})}}{m_{(\text{the total of AMM})}} \times 100\%$$

10 mL of DOX ethanol solution (1 mg/mL) was added to 10 mL of MONs-NH_2 ethanol solution (1 mg/mL), which mixed with 5 mL of genipin ethanol solution (1 mg/mL) at room temperature and stirred for 17 h. After centrifugation with ethanol wash for three times, the precipitate was collected and dispersed in water. 10 mL of the above solution (1 mg/mL) and 2 mL of CS aqueous solution (1 mg/mL) were stirred at room temperature for 6 h. After centrifugation and water washing for three times, the supernatant and precipitate were collected separately, and the precipitate was dispersed in ultrapure water and set aside. The preparation of DOX@AMM-Col was the same as that of the above method for the preparation of AMM-Col. The standard curve of DOX in ethanol was plotted and the DOX loading content (Loading content, %) and encapsulation efficiency (Encapsulation efficiency, %) were calculated. The calculation formula was as follows[8]:

$$\text{Loading content} = \frac{m_{(\text{the total of DOX})} - m_{(\text{the supernant of DOX})}}{m_{(\text{the total of DOX@AMM})}} \times 100\%$$

$$\text{Encapsulation efficiency} = \frac{m_{(\text{the total of DOX})} - m_{(\text{the supernant of DOX})}}{m_{(\text{the total of DOX})}} \times 100\%$$

5. The pH/GSH-responsiveness and photothermal properties

To evaluate the GSH responsive properties of AMM-Col, AMM-Col was reacted with GSH at 37 °C. After stirring for 4 h, TEM and DLS was carried out to observe the changes of morphology and size.

DOX release experiments were performed at different concentrations of GSH and pH. The dialysis bag was filled with 2 mL of DOX@AMM-Col (4 mg/mL), and 18 mL of PBS at different concentrations of pH and GSH were added to the external fluid of the dialysis bag. The concentration of DOX in the dialysate at different time points was determined using a UV-Vis absorption spectrum to plot the DOX release curve.

In order to investigate the photothermal effect of AMM-Col, AMM-Col with different concentrations (0.5, 1.0 and 2.0 mg/mL) were irradiated with NIR light (808 nm, 2.0 W/cm^2), the temperature change of the solutions was monitored within 10 min to plot the temperature curve. Then 1.0 mg/mL of AMM-Col was selected to be irradiated with different NIR power densities, the temperature change of the solution was monitored within 10 min to draw the temperature curve.

To verify the photothermal stability of AMM-Col, 1.0 mg/mL of AMM-Col was irradiated with NIR (3.0 W/cm^2) for 10 min, then NIR was removed to cooled for 10 min, where the cycle was repeated four times. During this process, the solution temperature change was recorded every 30 s to record and plot the cyclic curve of temperature.

6. Motility and collagenase activity

The motion of the nanomotor was recorded with CLSM. Firstly, 500 μL of 0.2 mg/mL of DOX@AMM-Col was taken in a 35 mm confocal dish and irradiated for 5 min at different NIR power densities (0, 1.0, and 2.0 W/cm^2) before being placed in the CLSM. The motion video was recorded at 10 fps using "xyt" mode with 100 frames each of 36.33 μm × 36.33 μm in size. The specific parameters were as follows: time interval of 551 ms, scanning speed of 2600 Hz, number of frames of 100, and size of each frame of 256 × 256 pixels. Fiji software was used to analyze the particle trajectories. The average velocity was obtained by averaging the particle velocities over different time intervals. A total of 15 different particles were selected for each set of samples to calculate the MSD values and to calculate the particle diffusion coefficient (Deff). The equation $MSD = (4 \times Deff)\Delta t + (v^2)(\Delta t^2)$ was used to fit the MSD curves. According to the equation $MSD = (4 \times Deff)\Delta t$, Deff can be extracted.[9]

The collagenase activity was assessed by using collagen gel containing FITC. Collagen was mixed with PBS containing FITC (10 μg/mL) in an ice bath, then the solution was moved to a 24-well plate and left at room temperature for 20 min to promote gelation. Once the gel was formed, wash the gel gently until negligible fluorescence was observed in the supernatant. Then 200 μL of PBS, Col, AMM-Col and AMM-Col + NIR were added to the gel surface, respectively, and the fluorescence in the supernatant was detected after incubation at 37°C for 24 h.[10]

The collagenase-dependent diffusion was assessed by measuring the diffusion coefficient by DLS[11] and the motility of AMM-Col dispersed in different concentrations of collagen solutions. where 1 mg of AMM-Col was dispersed in different concentrations of collagen solution (0, 0.5, 0.7 and 1.0 mg/mL).

7. *In vitro* biocompatibility and hemolysis tests

MTT assay: 5×10^3 cells (100 μL) of HL7702 cells and HepG2 cells were added to each well of a 96-well plate to incubate for 24 h. Gradient concentrations of AMM-Col and DOX@AMM-Col were added to further incubate for 24 and 48 h. After that, 100 μL of medium containing 0.5 mg/mL MTT was added to each well before incubation for 4 h. The medium with MTT was carefully aspirated from the wells and 100 μL of DMSO was added to each well to dissolved by shaking. Finally, the OD value was detected at 490 nm by an enzyme marker.

Hemolysis rate assay: Fresh mouse blood was processed by centrifugation to collect erythrocyte precipitates. DOX@AMM-Col and 0.5 mL of erythrocyte solution (1%) was mixed in equal volume. Meanwhile, negative controls (PBS) and positive (water) controls were established. The hemolysis rate was calculated as follows[12]:

$$\text{Hemolysis rate}\ (\%) = \frac{OD_t\text{-}OD_{nc}}{OD_{pc}\text{-}OD_{nc}} \times 100\%$$

Where the absorbance values of positive control, negative control and test samples were used to represent OD_{pc}, OD_{nc} and OD_t respectively.

8. *In vivo* fluorescence imaging

In order to track the distribution of nanomotors into the mouse body in organs, tumor-bearing mice (~100 mm^3) were subjected to optical imaging studies *in vivo*. 200 μL of DiO (Ex 646 nm, Em 663 nm) labelled AMM-Col was injected via the tail vein. The fluorescence distribution images of the mice were acquired by an *in vivo* 3D optical imaging system (IVIS Spectrum) at 0, 4, 8, 12, 18, 24, and 36 h after the injection, and the fluorescence intensities were analyzed by using Living Image software.

9. *In vivo* deep penetration and collagen content of tumor tissue

Tumor bearing mice (~100 mm^3) were established with PBS, NIR, DOX@AMM-Col, DOX@AMM-Col+NIR, and DOX@AMM-BSA+NIR groups, respectively. After 24 h of the last tail vein administration, the mice were executed and the tumor tissues were harvested. Frozen slides were prepared and stained with immunofluorescence (primary antibody: rabbit anti-mouse collagen type I antibody (Shanghai LMAI Bio Co., Ltd), secondary antibody: FITC-labelled sheep anti-rabbit IgG (Shanghai LMAI Bio Co., Ltd))[13]. Cell nuclei were stained with DAPI. Slides were observed by CLSM to take images, and the fluorescence intensity was subsequently analyzed by ImageJ software.

To assess the penetration and accumulation of nanomotors in the tumor tissue, AMM-Col was injected into the H22 cells-bearing mice via intravenous injection. The tumor area was irradiated with NIR light for 15 min after 12 h post-injection and the temperature of the tumor site was

recorded by an infrared thermal camera, and no NIR irradiation was used as a control.

10. The production of IFN-α, TNF-α and IL-6 *in vivo*

Type I interferon (IFN-α) and cytokine secretion (TNF-α and IL-6) in tumor was assessed. The supernatant from the tumor after grinding and centrifugation in the above experiments was collected, where the levels of IFN-α, TNF-α, and IL-6 were measured using ELISA kits (Hefei Laier Biotechnology Co., Ltd).

11. The immune cell infiltration *in vivo*

The infiltration of immune cells in the tumor was assessed. The mice were randomly divided into five groups (n = 5), namely PBS, AMM-Col, AMM-Col+NIR, DOX@AMM-Col and DOX@AMM-Col+NIR groups, when the tumor volume reached 100~150 mm^3. Then 100 μL of PBS, AMM-Col (7.34 mg/mL), AMM-Col (7.34 mg/mL), DOX@AMM-Col (8.34 mg/mL), and DOX@AMM-Col (8.34 mg/mL) were administered to the above groups via the tail vein on days 0 and 3, respectively, where AMM-Col+ NIR and DOX@AMM-Col+NIR groups subjected the mice to NIR light treatment for 5 min (1.5 W/cm^2) after 12 and 14 h of drug administration. Mice were executed and dissected to obtain tumor tissues after 24 h of the last dose, which were subsequently ground and filtered through a 70 μm cell strainer to collect single-cell suspensions. The obtained single-cell suspensions were centrifuged, resuspended, and counted, stained by the flow antibody. Finally, the cells were resuspended with 0.3 mL of PBS and detected by flow cytometry. Flow antibodies anti-mouse CD3-PE, anti-mouse CD45-FITC and anti-mouse CD8-APC were used to stain cytotoxic T lymphocytes (CTL); anti-mouse CD45-FITC, anti-mouse CD11c-PE and anti-mouse MHC II-APC were used to stain dendritic cells (DC).

12. Anti-tumor evaluation *in vivo*

Tumor bearing mice (~100 mm^3) were randomly divided into five groups (n = 5), namely PBS, AMM-Col, AMM-Col+NIR, DOX@AMM-Col and DOX@AMM-Col+NIR groups. Then 100 μL of PBS, AMM-Col (7.34 mg/mL), AMM-Col (7.34 mg/mL), DOX@AMM-Col (8.34 mg/mL), and DOX@AMM-Col (8.34 mg/mL) were administered to the above groups via the tail vein on days 0 and 3, respectively, where AMM-Col+ NIR and DOX@AMM-Col+NIR groups subjected the mice to NIR light treatment for 5 min (1.5 W/cm^2) after 12 and 14 h of drug administration. Tumor volume and body weight were monitored once a day during the treatment period and recorded against, and the tumor volume was calculated as follows[14]:

$$\text{Tumor volume } (mm^3) = \frac{\text{length} \times \text{width}^2}{2}$$

13. Histological examination

Following the anti-tumor experiments, the mice were executed and dissected, where the tumors were removed for weighing and photographing, while the major organs (heart, liver, spleen, lungs and kidneys) were collected for fixation in Bouin's solution, then washed by graded ethanol solutions (50, 60, 70%) after 24 h and subsequently stored in 75% ethanol. Paraffin slides were prepared and stained with hematoxylin-eosin (H&E) to observe the damage and cellular morphology of the tumor tissues and major organs.

14. Movies S1-S5

Movie S1: AMM-Col in water with NIR at 0 W/cm^2.

Movie S2: AMM-Col in water with NIR at 1 W/cm^2.

Movie S3: AMM-Col in water with NIR at 2 W/cm^2.

Movie S4: AMM-Col in collagen solution (0.5 mg/mL).

Movie S5: AMM-Col in collagen solution (1 mg/mL).

Movie S6: AMM-Col in collagen solution (1 mg/mL) with NIR at 0 W/cm^2.

Movie S7: AMM-Col in collagen solution (1 mg/mL) with NIR at 2 W/cm^2.

15. Figure S1-S14

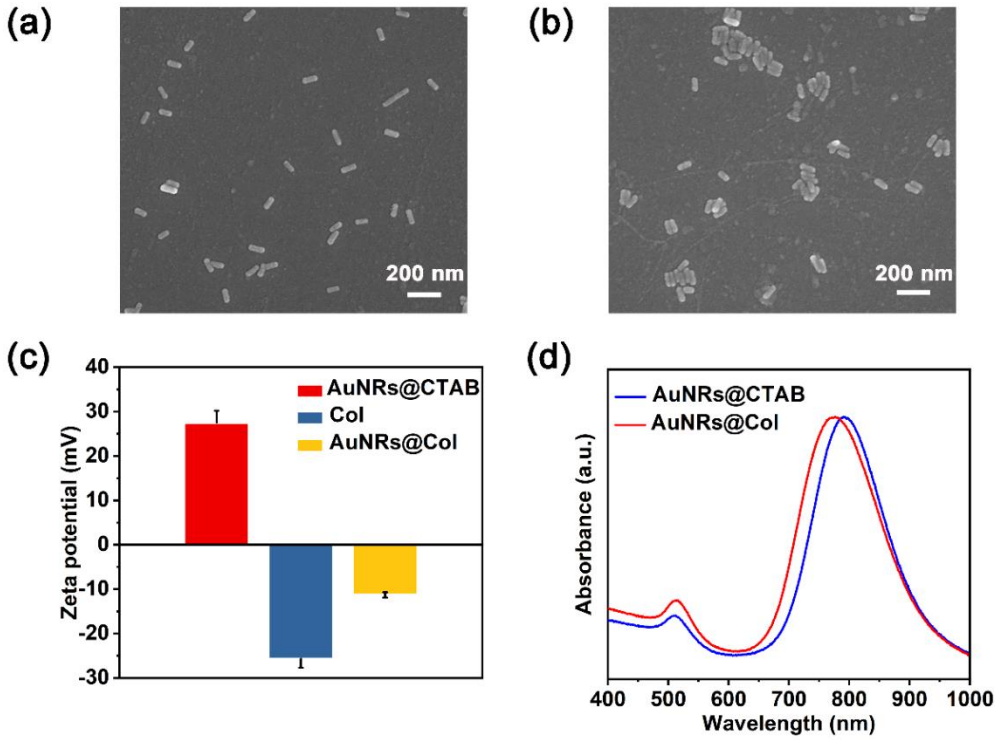

Fig. S1 SEM image of (a) AuNRs@CTAB and (b) AuNRs@Col; (c) Zeta potential of AuNRs@CTAB, Col, and AuNRs@Col (n = 3); (d) UV-Vis spectra of AuNRs@CTAB and AuNRs@Col. AuNRs stabilized by CTAB (AuNRs@CTAB) were prepared by seed growth method[1], followed by the replacement of CTAB with Col by ligand exchange method to yielding AuNRs@Col[15]. As shown in Fig.S1a, the scanning electron microscope (SEM) image indicated that AuNRs@CTAB was a rod-like morphology with a length of *ca.* 70 nm and a width of *ca.* 10 nm. The

morphology of AuNRs@Col was shown to be also the rod-like structure in SEM image (Fig.S1b), where the surface morphology of AuNRs@Col became rougher compared with AuNRs@CTAB, indicating initially that AuNRs were successfully modified by Col. In addition, the zeta potential changed from +27.5 mV to -11.3 mV (Fig.S1c), further demonstrating the successful preparation of AuNRs@Col. Notably, the modification of Col had no effect on the maximum absorption wavelength of AuNRs (Fig.S1d), which suggests that the gold nanorods are capable of utilizing 808 nm NIR light to activate their photothermal activity in subsequent applications.

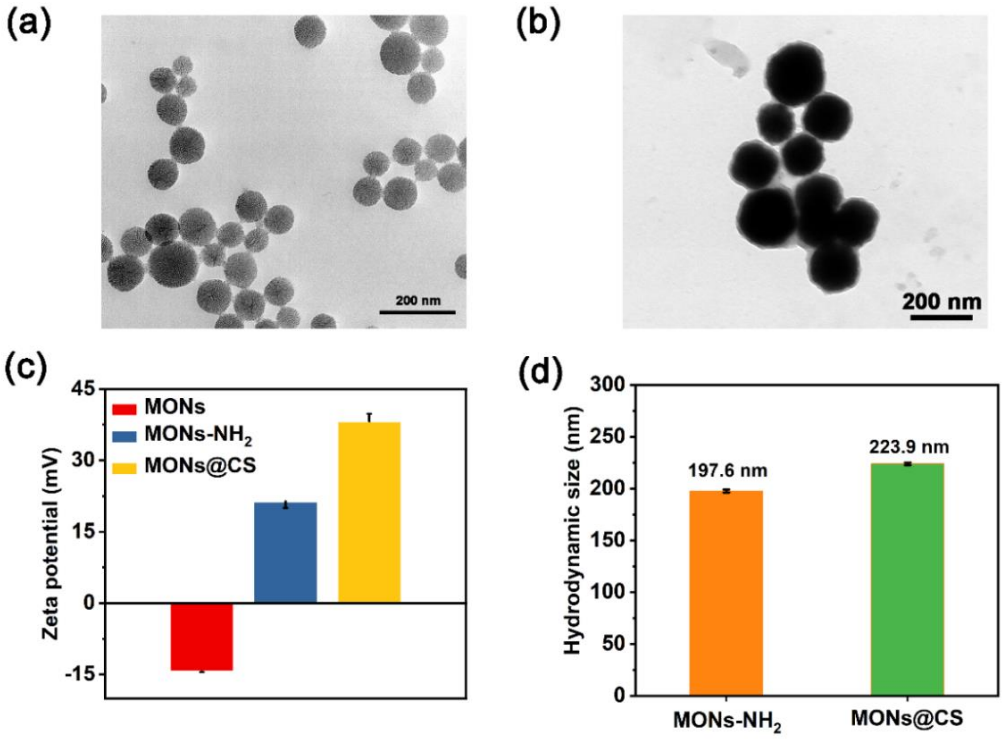

Fig. S2 TEM images of (a) MONs-NH_2 and (b) MONs@CS; (c) Zeta potential of MONs, MONs-NH_2, and MONs@CS (n = 3); (d) the average hydrodynamic size of MONs-NH_2 and MONs@CS (n = 3). The CTAB-mediated sol-gel method was used to synthesize tetrasulfur bond-containing MONs[3], followed by the preparation of surface-amidated MONs (MONs-NH_2) by reaction with APTES.[4] As shown in Fig. S2a, transmission Electron Microscope (TEM) image indicated that MONs-NH_2 was spherical morphology with an average diameter of *ca.* 140 nm. The zeta potential changed from -14.4 mV to +21.4 mV (Fig. S2c)[6], revealing the success in surface amination. The surface of MONs-NH_2 was further modified by CS via the cross-linking agent genipin (GNP) to prepare MONs@CS.[16] As shown in Fig.S2b, a clear film modification on the surface of MONs@CS was observed, which initially proved the successful coating by CS. The further increase in zeta potential to +38.2 mV (Fig. S2c) resulting from the abundant amino groups on CS was also demonstrated that the successful coating by CS[5]. Moreover, as shown in Fig. S2d, the average hydrodynamic diameter of MONs@CS increased from 197.6 nm of MONs-NH_2 to 223.9 nm, further confirming the successful preparation of MONs@CS.

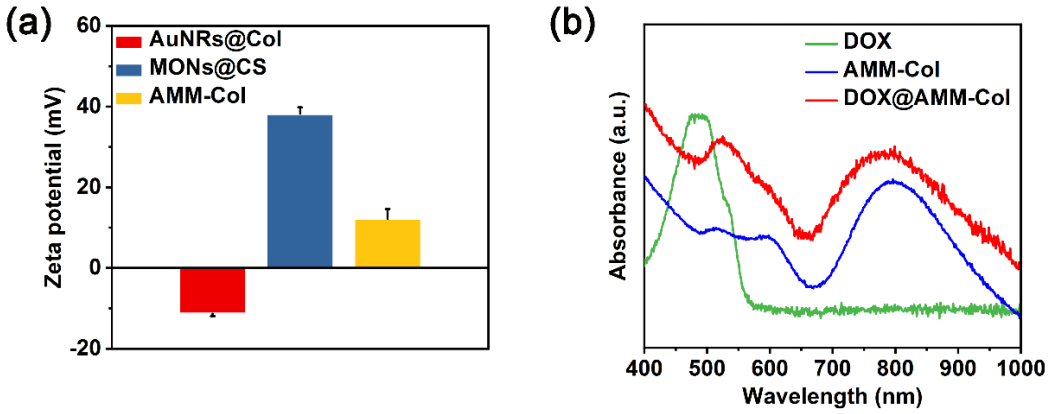

Fig. S3 (a) Zeta potential AuNRs@Col, MONs@CS, and AMM-Col (n = 3); (b) UV-Vis spectra absorption of DOX，AMM-Col and DOX@AMM-Col.

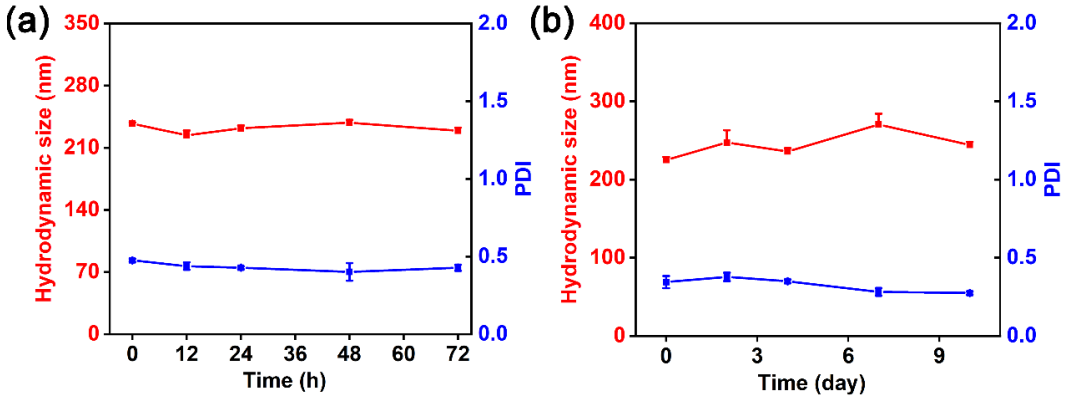

Fig. S4 The average hydrodynamic diameter of AMM-Col in complete 1640 medium with 10% FBS (a) and PBS (pH 7.4) (b). DOX@AMM-Col remained stable in 1640 medium containing 10% FBS for 72 h with no significant variation in particle size. The particle size of DOX@AMM-Col in PBS (pH 7.4) could maintain good stability and no decomposition within10 days. These finding indicated good colloidal stability in physiological conditions (n = 3).

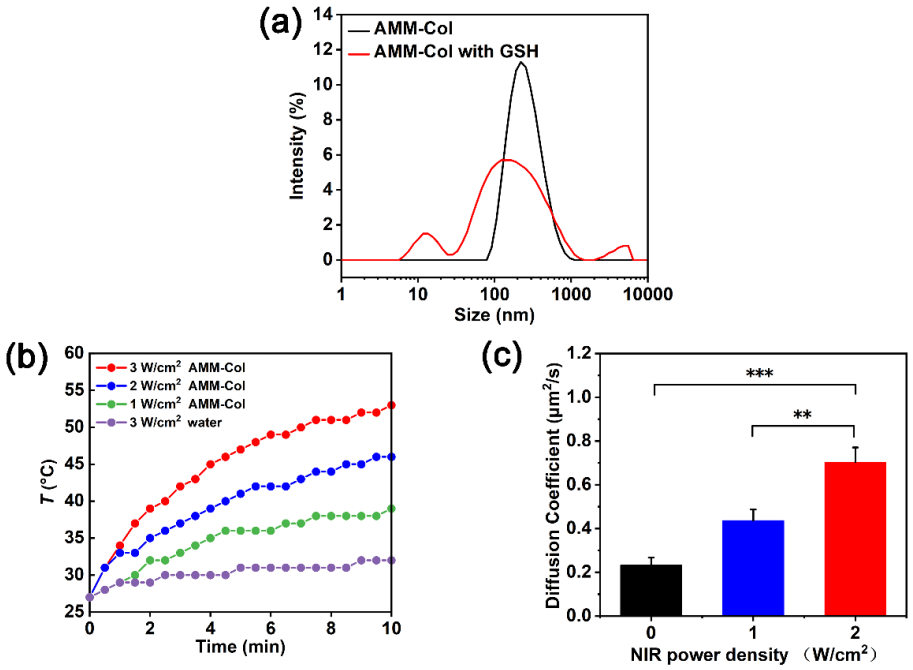

Fig. S5 (a) The hydrodynamic size of AMM-Col before and after GSH; (b) photothermal performance of AMM-Col at different NIR powers with the same concentration; (c) the diffusion coefficient of AMM-Col under different NIR power (n = 3).

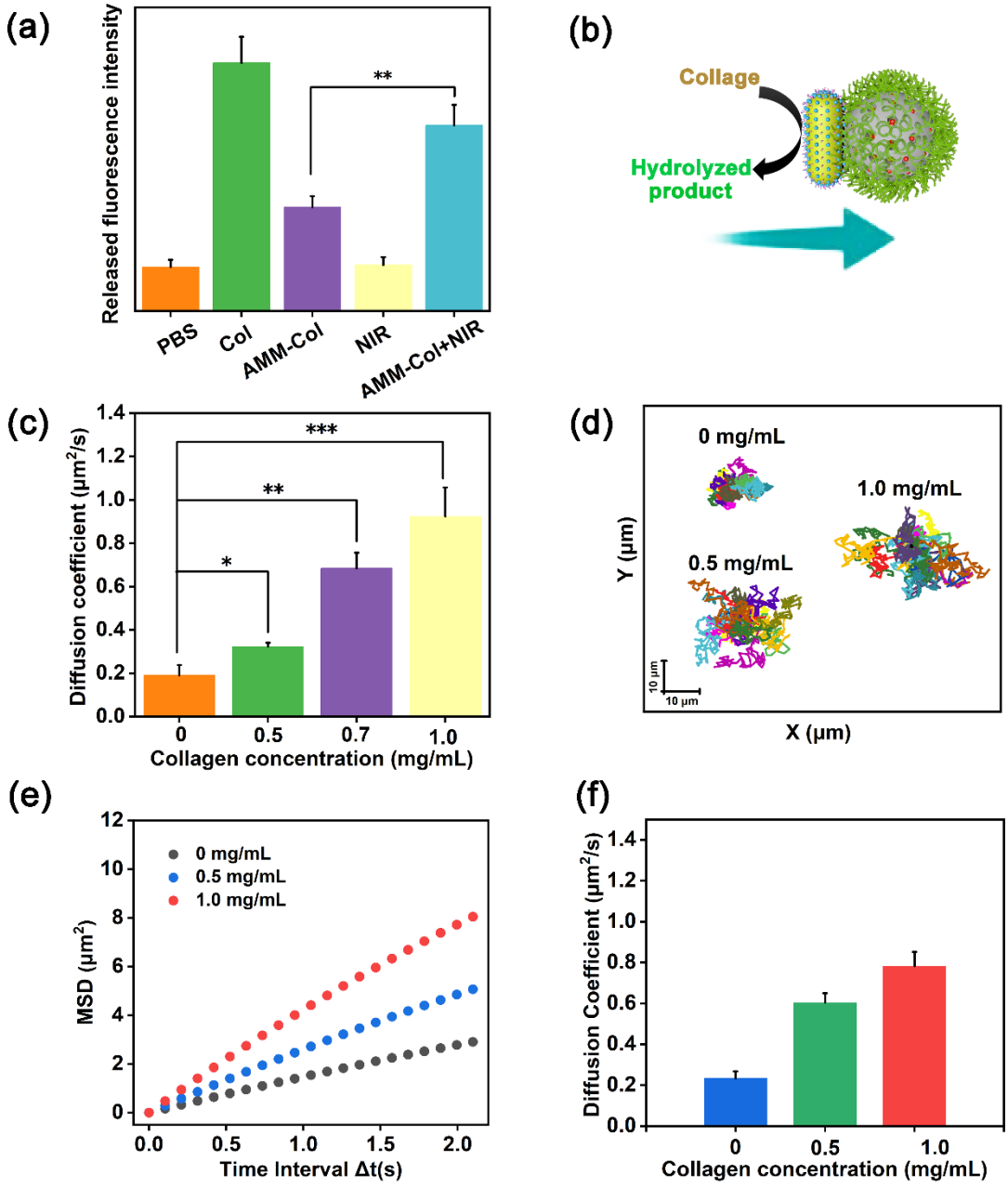

Fig. S6 (a) Fluorescein released by a FITC-containing collagen matrix treated with PBS, Col, AMM-Col, and AMM-Col+NIR. Collagen gel containing FITC was used to study the enzymatic activity.[10] When the gel was treated with Col, the FITC within the gel was released due to collagen degradation. Thus, the fluorescence intensity in the supernatant can reflect the efficacy of collagen degradation of the preparation, where the supernatant of the PBS had only slight fluorescence intensity, which might have been due to a small amount of FITC present on the gel surface. In contrast, the fluorescence intensity of AMM-Col was significantly higher than that of the PBS, showing that AMM-Col could effectively degrade collagen gel and release FITC. In addition, the FITC fluorescence intensity released in the AMM-Col+NIR treated gels was significantly higher than that of AMM-Col, indicating that NIR-

triggered photothermal effects could activate effectively Col activity to degrade collagen. Notably, NIR light had no effect on collagen degradation; (b) Col on AMM-Col catalyses collagen to produce asymmetric concentration gradients of hydrolysis products triggering motility of AMM-Col as a self-diffusiosphoresis; (c) the diffusion coefficient of AMM-Col in different concentrations of collagen protein solutions measured by DLS (n = 3); (d) the motion trajectories of AMM-Col in various collagen solution (Movie S1, S5, and S6), and the corresponding (e) MSD and (f) diffusion coefficient (n = 15). The product concentration gradients can be generated by enzymatic reactions due to the asymmetric distribution of Col on AMM-Col, which triggered AMM-Col movement in the form of self-diffusiosphoresis with substrate concentration-dependent movement properties (Fig. S6b). Therefore, the diffusion coefficient of AMM-Col in various collagen substrate concentrations was first tested by DLS, where results showed that the diffusion coefficient increased with increasing collagen substrate concentration (Fig. S6c). In addition, Col-dependent diffusion was further evaluated by CLSM. As shown in Fig. S6d, the diffusion trajectory was significantly lengthened with increasing collagen substrate concentrations. Meanwhile, the corresponding MSD analysis (Fig. S6e) and diffusion coefficient (Deff = MSD/4Δt) (Fig. S6f) was further supported the above results. These results indicated that AMM-Col was capable of collagenase-dependent diffusion.

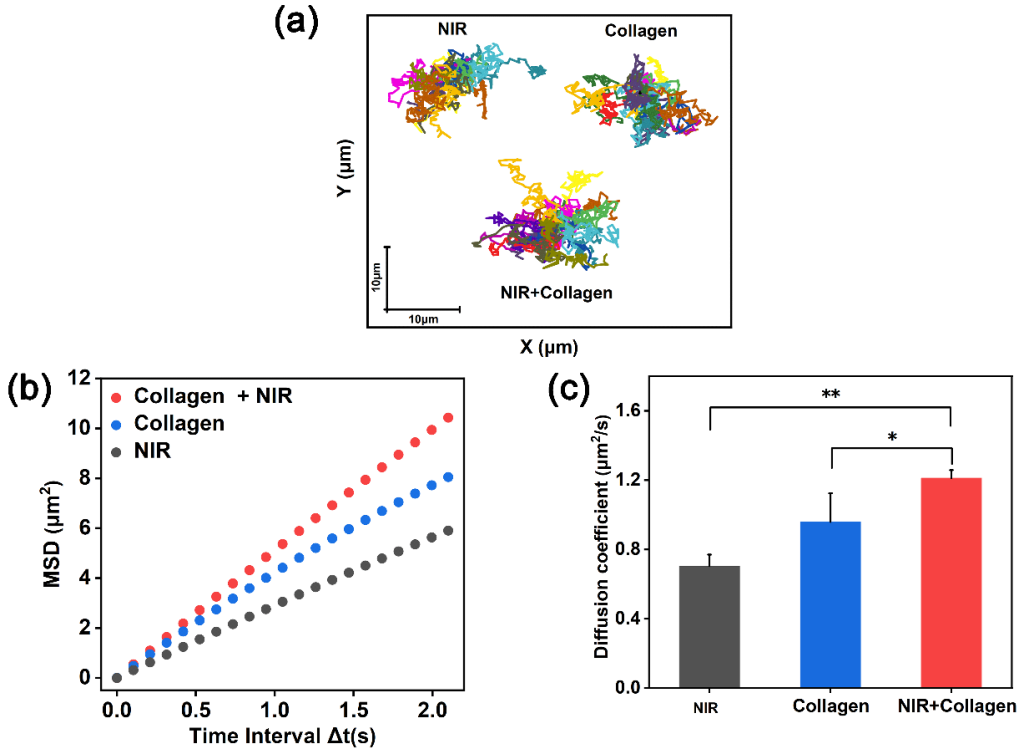

Fig. S7 (a) The motion trajectories of AMM-Col in PBS solution under NIR, AMM-Col in collagen solution without NIR, and AMM-Col in collagen solution under NIR (Movie S3, S7, and S8); The corresponding (b) MSD and (c) diffusion coefficient (n = 15). The diffusion trajectory of AMM-Col under NIR was enhanced compared to AMM-Col, indicating that NIR-triggered photothermal effects could activate effectively collagenase activity. Meanwhile, the corresponding enhanced MSD and diffusion coefficient was further supported the above results.

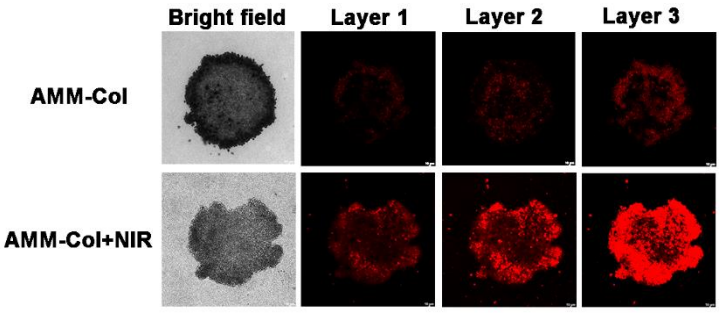

Fig. S8 Cross-sectional CLSM images of Cy5.5-labeled AMM-Col at different thickness intervals from the top to bottom of the 3D MTS with *ca.* 120 μm height. Three layers represent 1/6, 1/3, and 1/2 thickness, respectively.

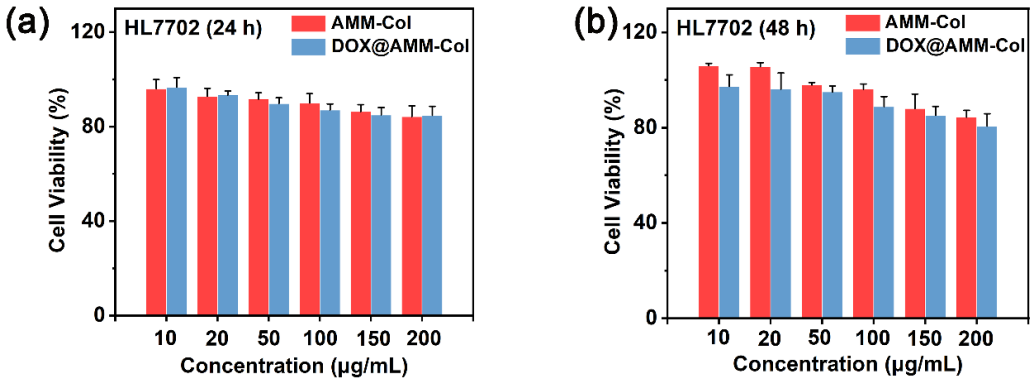

Fig. S9 Cytotoxicity of HL7702 cells further incubated for 24 and 48 h after NIR at a power density of 0.5 W/cm^2 for 5 min; cytotoxicity of HL7702 cells incubated with AMM-Col and DOX@AMM-Col in different concentrations (b) 24 h and (c) 48 h. (n = 6).

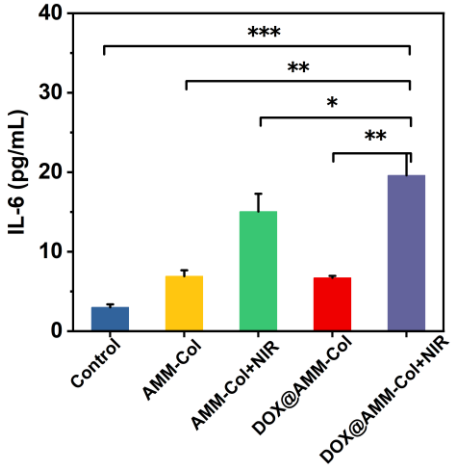

Fig. S10 ELISA kits assessed the secretion levels of inflammatory factors IL-6 in tumor (n = 3).

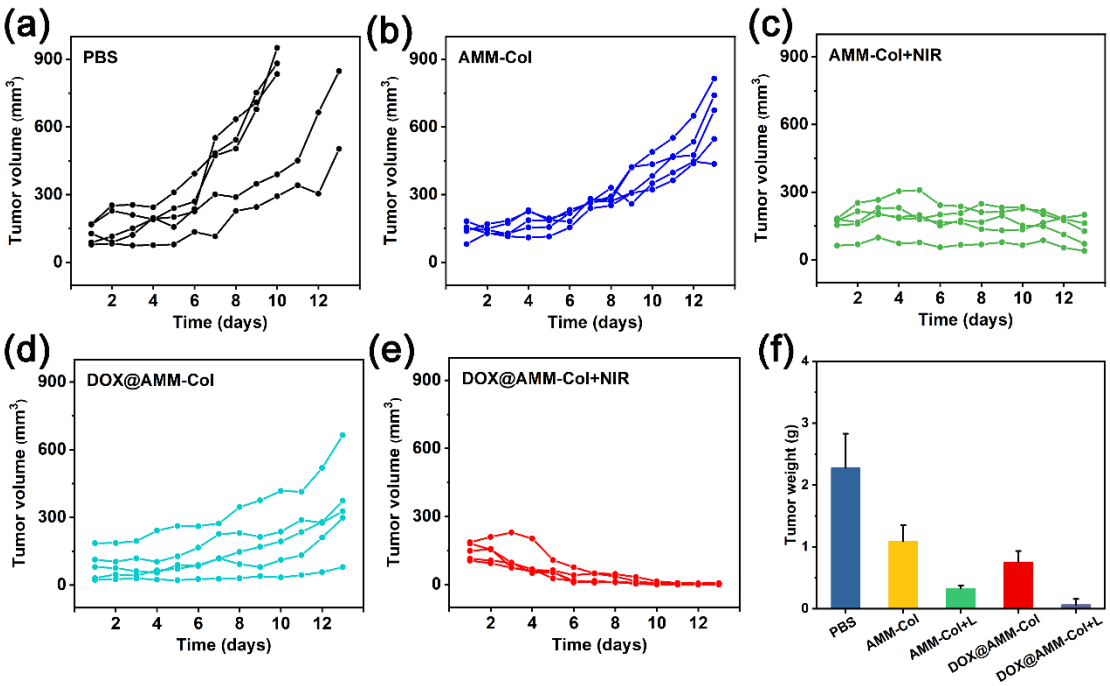

Fig. S11 (a-e) mouse tumor growth curves with different treatment groups (n = 5); f) the weight analysis of isolated tumor tissue (n = 5).

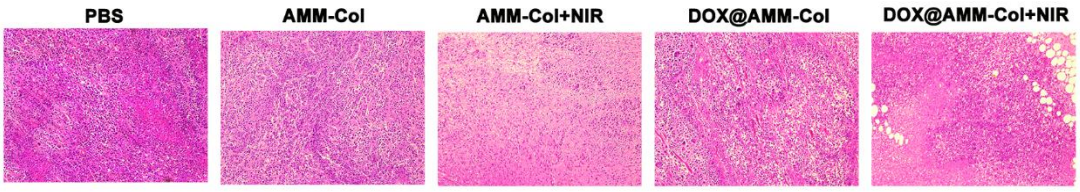

Fig. S12 The tumor section images of H&E stained from each group of mice.

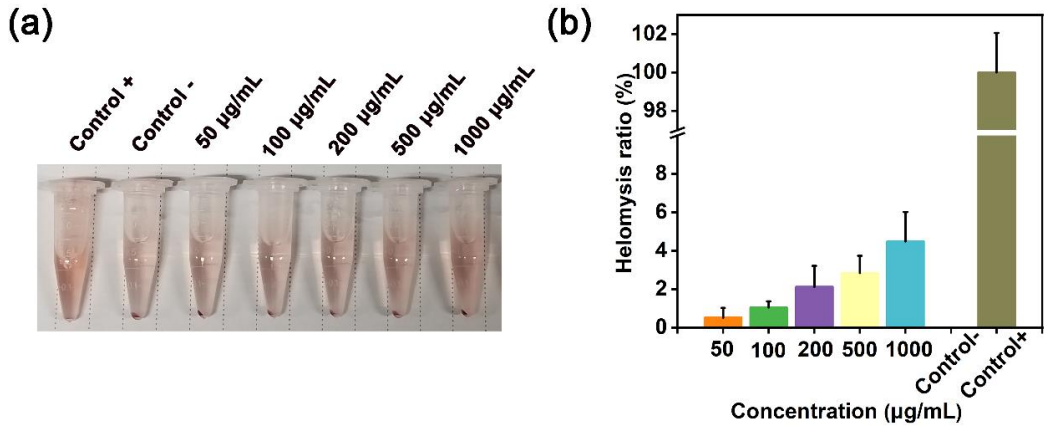

Fig. S13 The hemolysis assay (a) and hemolysis rate (b) of DOX@AMM-Col (n = 3).

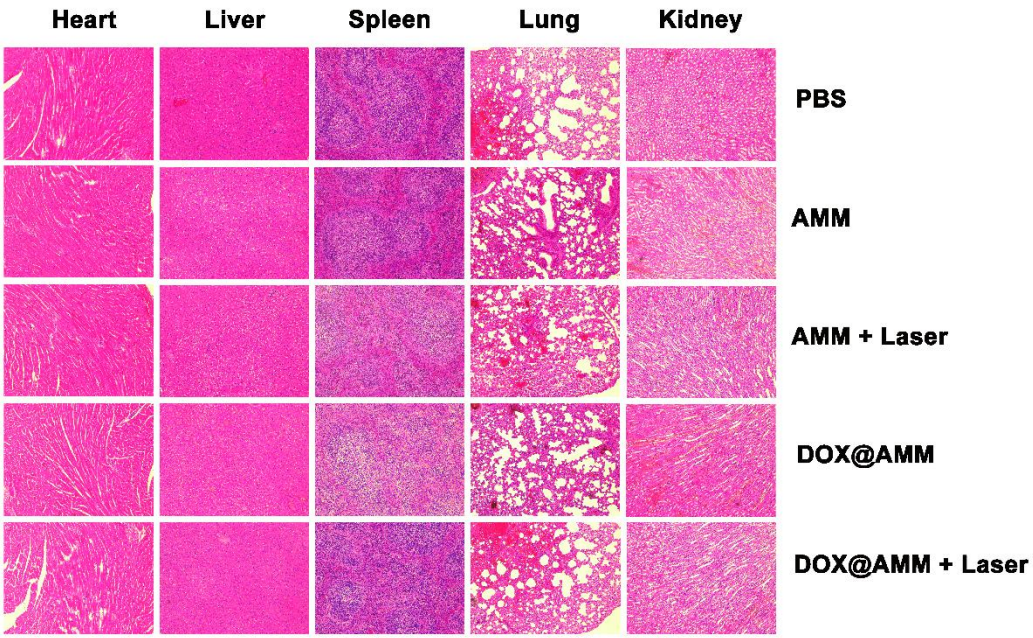

Fig. S14 H&E staining images of major organs from different groups.

16. References

1. Y. Wang, Y. F. Wen, Y. Qu, Z. C. Pei and Y. X. Pei, *J. Colloid Interf. Sci.*, 2022, **615**, 386-394.
2. X. K. Jin, H. Yang, Z. W. Mao and B. Wang, *J. Colloid Interf. Sci.*, 2021, **601**, 714-726.
3. Y. L. Zhang, M. Dang, Y. Tian, Y. F. Zhu, W. F. Liu, W. Tian, Y. Y. Su, Q. Q. Ni, C. L. Xu, N. Lu, J. Tao, Y. J. Li, S. Zhao, Y. Zhao, Z. L. Yang, L. Sun, Z. G. Teng and G. M. Lu, *ACS Appl. Mater. Interf.*, 2017, **9**, 30543-30552.
4. Y. N. Liu, L. Xie, M. Gao, R. H. Zhang, J. C. Gao, J. D. Sun, Q. D. Chai, T. Wu, K. Liang, P. Chen, Q. Wan and B. Kong, *ACS Appl. Mater. Interf.*, 2021, **13**, 50246-50257.
5. K. Ma, Y. B. Cheng, X. R. Wei, D. J. Chen, X. L. Zhao and P. X. Jia, *J. Biomater. Appl.*, 2021, **35**, 857-868.
6. R. H. Jin, Z. N. Liu, Y. K. Bai, Y. S. Zhou, J. J. Gooding and X. Chen, *Adv. Funct. Mater.*, 2018, **28**, 1801961.
7. H. Y. Huang, L. Q. Chen, W. Sun, H. H. Du, S. L. Dong, A. M. Q. Ahmed, D. Y. Cao, J. H. Cui, Y. Zhang and Q. R. Cao, *Theranostics*, 2021, **11**, 906-924.
8. J. L. Dong, Y. Y. Yu, Y. X. Pei and Z. C. Pei, *J. Colloid Interf. Sci.*, 2022, **607**, 1651-1660.
9. S. P. Cao, H. L. Wu, I. A. B. Pijpers, J. X. Shao, L. K. E. A. Abdelmohsen, D. S. Williams and J. C. M. van Hest, *ACS Nano*, 2021, **15**, 18270-18278.
10. X. Y. Yang, J. G. Zhang, Q. M. Zhou, J. N. Yu, Y. F. Lu, X. J. Wang, J. P. Zhou, X. F. Ding, Y. Z. Du and R. S. Yu, *J. Nanobiotechnol.*, 2022, **20**, 524.

11. Y. C. Ye, F. Tong, S. H. Wang, J. M. Jiang, J. B. Gao, L. Liu, K. Liu, F. Wang, Z. Wang, J. F. Ou, B. Chen, D. A. Wilson, Y. F. Tu and F. Peng, *Nano Lett.*, 2021, **21**, 8086-8094.
12. Z. C. Liu, S. P. Liu, X. Y. Zhao, C. L. Xue, Y. Liu and Q. Shuai, *Int. J. Biol. Macromol.*, 2023, **240**, 124486.
13. M. M. Wan, H. Chen, Z. Wang, Z. Y. Liu, Y. Q. Yu, L. Li, Z. Y. Miao, X. W. Wang, Q. Wang, C. Mao, J. Shen and J. Wei, *Adv. Sci.*, 2021, **8**, 2002525.
14. Y. Wang, Z. L. Chen, J. H. Li, Y. F. Wen, J. X. Li, Y. H. Lv, Z. C. Pei and Y. X. Pei, *Adv. Sci.*, 2024, **11**, 2306178.
15. J. Meena, A. Gupta, R. Ahuja, M. Singh and A. K. Panda, *J. Mol. Liq.*, 2021, **338**, 116602.
16. F. Emadi, A. Amini, A. Gholami and Y. Ghasemi, *Sci. Rep.*, 2017, **7**, 42258.